2005 WJTA American Waterjet Conference
August 21-23, 2005 • Houston, Texas

Paper 3A-4

STUDY ON THE TEMPERATURE DISTRIBUTIONS OF WATER JET BY INFRARED THERMAL TESTING AND IMAGE PROECSSING TECHNOLOGY

Cui Longlian Gong Weili An Liqian
School of Mechanics, Architecture & Civil Engineering
China University of Mining and Technology
Beijing, P.R. China

ABSTRACT

This paper presents a study on using the infrared thermal imager to obtain the temperature distributions of water jet, and from which the mathematical models of the jet flow were obtained, with the help of theoretical analysis.

An experiments using infrared thermal imager were conducted for the Infrared thermal images of the water jet flow. Through infrared thermal images denoising and data fitting, isotherm of the water jet and the temperature variation curve of different distance form the nozzle outlet were obtained. In order to calculate the shear stress within the boundary layers, multi-phase models have been developed. The numerical computation was used to get the velocity and temperature distribution of the water jet.

The infrared images were transformed to temperature distribution by image processing technology. The analyses were made to obtain the relationships between the temperature distributions under pump pressure. The results indicate that the temperature distribution was similar when the pump pressure greater than the threshold pressure, which was proved by the further theoretical computation and experiments data. The temperature distribution from experiments is in good agreement with the temperature distribution from theoretical result.

1. INTRODUCTION

High pressure water jet technology achieved significant progress during last decades in applications such as cutting and comminuting of wide range of materials, surface cleaning and removal of surface layers, and repair of concrete structures. Mangy reports have been written describing the velocity and pressure distribution and efficiency of water jet namely Humio (1990), Shimizu (1992), Bhra (1988). Masatoshi et al. (1996) used the custom-designed device to measure both the water jet's speed and pressure distribution in an attempt to clarity the actual structure of a water jet. Hlaváč et al (1999) deduced simple quick method to confirm speed and pressure distribution of the axial symmetrical supersonic water jet through summarizing theory and experiment. Though the velocity and pressure distributions of water jet were presented in many papers, few papers concerned the energy and temperature distribution of water. To make better use of the water jet energy, we should know more detailed characteristics of the water jet. The paper presents a study using the infrared thermal imager to get the temperature field of water jet; it is identical to the result from the theoretical analysis and numerical solutions.

2. MATHEMATICAL MODELS

2.1 Governing Equations

Under considering of the air influences, in order to study the distribution of temperature and velocity distribution in water jet□the multiphase models were applied to describing the fluid flow. Liu (2002) used the computational fluid dynamic (CFD) to simulation the fluid flow of abrasive water jet and obtained satisfactory results, where the multiphase model was employed. In cylindrical coordinates, the standard k-ε model was used, the relevant equations are present under the flowing assumption: The flow is steady state, turbulent, incompressible, two-phase flow.

$$\frac{\partial \rho_w \alpha_w u}{\partial x} + \frac{1}{r}\frac{\partial r \rho_w \alpha_w v}{\partial r} = 0 \qquad (1)$$

$$\frac{\partial \rho_g \alpha_g u}{\partial x} + \frac{1}{r}\frac{\partial r \rho_g \alpha_g v}{\partial r} = 0 \qquad (2)$$

$$\alpha_w + \alpha_g = 1 \qquad (3)$$

$$\rho = \alpha_g \rho_g + \alpha_w \rho_w \qquad (4)$$

$$\frac{\partial \rho uu}{\partial x}+\frac{1}{r}\frac{\partial r\rho vu}{\partial r}=-\frac{\partial P}{\partial x}+2\frac{\partial}{\partial x}\left(\mu_{eff}\frac{\partial u}{\partial x}\right)+\frac{1}{r}\frac{\partial}{\partial r}\left(r\mu_{eff}\left(\frac{\partial u}{\partial r}+\frac{\partial v}{\partial x}\right)\right) \quad (5)$$

$$\frac{\partial \rho uv}{\partial x}+\frac{1}{r}\frac{\partial r\rho vv}{\partial r}=-\frac{\partial P}{\partial r}+\frac{\partial}{\partial x}\left(\mu_{eff}\left(\frac{\partial v}{\partial x}+\frac{\partial u}{\partial r}\right)\right)+2\frac{1}{r}\frac{\partial}{\partial r}\left(r\mu_{eff}\frac{\partial v}{\partial r}\right)-2\frac{\mu_{eff}v}{r^2} \quad (6)$$

$$\frac{\partial \rho uT}{\partial x}+\frac{1}{r}\frac{\partial r\rho vT}{\partial r}=\frac{\partial}{\partial x}\left(\left(\frac{\mu_1}{\Pr}+\frac{\mu_t}{\sigma_t}\right)\frac{\partial T}{\partial x}\right)+\frac{1}{r}\frac{\partial}{\partial r}\left(r\left(\frac{\mu_1}{\Pr}+\frac{\mu_t}{\sigma_t}\right)\frac{\partial T}{\partial r}\right)+G_k \quad (7)$$

$$\frac{\partial \rho uk}{\partial x}+\frac{1}{r}\frac{\partial r\rho vk}{\partial r}=\frac{\partial}{\partial x}\left(\left(\mu_1+\frac{\mu_t}{\sigma_k}\right)\frac{\partial k}{\partial x}\right)+\frac{1}{r}\frac{\partial}{\partial r}\left(r\left(\mu_1+\frac{\mu_t}{\sigma_k}\right)\frac{\partial k}{\partial r}\right)+G_k-\rho\varepsilon+D \quad (8)$$

$$\frac{\partial \rho u\varepsilon}{\partial x}+\frac{1}{r}\frac{\partial r\rho v\varepsilon}{\partial r}=\frac{\partial}{\partial x}\left(\left(\mu_1+\frac{\mu_t}{\sigma_\varepsilon}\right)\frac{\partial \varepsilon}{\partial x}\right)+\frac{1}{r}\frac{\partial}{\partial r}\left(r\left(\mu_1+\frac{\mu_t}{\sigma_\varepsilon}\right)\frac{\partial \varepsilon}{\partial r}\right) \quad (9)$$
$$+\left(C_1 f_1 G_k-C_2 f_2\rho\varepsilon\right)/k+E$$

Equations (1) and (2) are the continuity, equations (5) and (6) are the momentum equations for axial and radial flow respectively. Equations (7) to (9) are the energy equation, kinetic energy equation of the turbulence and dissipative equation of turbulence. Subscripts w, g, are used for water, and gas flow variables respectively. G_k is the term of viscosity dissipation, mathematical expression given by

$$G_k=\mu_t\left\{2\left[\left(\frac{\partial u}{\partial x}\right)^2+\left(\frac{\partial v}{\partial r}\right)^2+\left(\frac{v}{r}\right)^2\right]+\left(\frac{\partial v}{\partial x}+\frac{\partial u}{\partial r}\right)^2\right\}, \quad D=0, \quad E=0$$

Where μ_t is coefficient of turbulent viscosity and μ_{eff} is effective coefficient of viscosity were given by

$$\mu_t=\rho C_\mu f_\mu k^2/\varepsilon$$

And $\mu_{eff}=\mu_1+\mu_t$

Where C_μ, C_1 and C_2 are constant, and σ_k and σ_ε are the turbulent Prandtl numbers for k and ε respectively. Launder (1972) provide the value of these constants in his book, C_μ=0.09, C_1=1.44, C_2=1.92, σ_k=1.0 andσ_ε=1.3.

Liu (2004) and Wang (2003) had presented the boundary condition in their paper and book. Control volume being used to discrete the equations, and the numerical solutions were obtained

by SIMPLE algorithm, Patankar (1980) gave the more detail about the processed of solving equation in his books.

3. EXPERIMENT

3.1 Experiment Principle

It is well known that the high-pressure pump does work to water which make the water have kinetic energy. During the water flowing in the pipe and issuing from the nozzle, because of the friction, there will be has some kinetic energy of water jet change into heat, which makes the temperature of water jet rise. There are have temperature difference between the water jet and ambient air, speed and temperature boundary layer formed on the interfaces of water jet and ambient air. The mass and heat transfer generated on the boundary layer.

In order to study the real-time heat transfer on the boundary layer, Infrared thermal imager was used. The advantage of the infrared thermal imager is that it can get images and data accurately, real-time, quickly and continuously. It has been widely used in many fields, in spite of some researchers (Kovacevic, Mohan, Beardsley, 1996) had used infrared thermal imager to study the generated heat and thermal energy distribution through the work piece during cutting with an abrasive water jet. However, it is the first time used for experimentation on the temperature distributions of the water flow.

3.2 Experimental Apparatus

Figure 1 is a schematic of our experimental setup which includes two parts, the first part is device which can produce high velocity water jet, and the second part is dark chamber and infrared thermal imager. As we known that visible light and the heat source can produce heavy influence to experiment, make experimental errors become heavy. In order to reduce the experimental errors, we have taken the following measures: the experiment was carried on the evening, nozzle and infrared thermal imager were placed in the dark chamber, separated a long distance between the pump and the dark chamber. The type of the infrared thermal imager is MK8100-II high sensitivity infrared thermal imager, its sensitivity is 0.025ºC and the available scope of temperature is from -40ºC to 300ºC.

In the experiments, rated pressure of the high pressure pump is 70MPa, and the pressure being used in the experiments was 2Mpa, 10MPa, 16MPa, 20MPa, 26MPa, 30MPa and 36MPa.The range of the infrared thermal imager was set from 19ºC to 24ºC, and its sensitivity is 0.025ºC, the speed of gathered the infrared thermal images was 6 pictures pre second, 128 pictures were gathered under each of different pressures.

4. RESULTS AND DISCUSSION

4.1 Characteristics of the Temperature Profile

Typical temperature distributions from the experimental and numerical solutions are shown in Figure 2(a) and Figure 2(b) respectively. Analyzing the experimental results and numerical results for the temperature distribution of the water jet has shown that the experimental results and the numerical solutions are identical basically. But the experimental results can not reveal the temperature distributions of the water jet core, the reasons is attributed to the higher temperature water jet core was surrounded by the low temperature water which made the infrared radicalization of the higher temperature water jet core could not be detected.

It can be seen from the Figure 2 that the peak temperature is always in the jet centre, and the temperature decrease along the jet in axial and radial direction, mainly because of air entrainment which made the heat transfer from the water to the air through convention and conduction.

Figure 3 shows the profile of the temperature in the jet axial direction. It can be seen from the Figure 3 that the peak temperature is always in the jet centre, and the temperature decrease along the jet in axial and radial direction, mainly because of air entrainment which made the heat transfer from the water to the air through convention and conduction.

Figure 4 shows the profile of the temperature in the radial direction at the different cross-sections of x=10, 40, 70 mm from the nozzle. It can be seen that the jet temperature decreases as the radial from the jet centre increase in all the three cross-sections considered. The temperature decrease are similarity in the first two cross-section when the radial distance within 5mm, and the temperature decrease is relatively small when the radial distance is exceed 5mm. Compare the third cross-section x=70 with the first two cross-section, the temperature decrease is gradual and the temperature of the jet's outer layer is higher.

There have some differences between Figure 4(a) and Figure 4(b) as following: in the experimental data Figure 4(a) the temperature profile in the third cross-section is not symmetry and the range with higher temperature in the middle of the third cross-section is wider than Figure 4(b). In the first two cross-sections when the radial distance exceeds 5 mm, the trend of temperature vary is decrease with fluctuation in Figure 4(a), but the temperature keeps as a constant in Figure 4(b). Using the infrared thermal imager collected data real-time, the randomness on the time and space distribution of the water jet turbulence were shown. This is the mainly reasons for the difference between the experimental data and numerical solutions.

4.2. Pressure Variety and the Temperature Profile

Figure 5 show the temperature distribution of the jet under the difference pressure of 2MPa, 10MPa and 30MPa. It can be seen that the scope of temperature profile become lager as the pressure increase. In Figure 5(a) the temperature is invariability in axial and radial direction, the irregularity curves in outside is the borderline curve of the air, the gray line is the shape of the water jet, the change of water jet's diameter is not obvious in the direction. Figure 5 (b), (c) demonstrate that the temperature decrease is faster in radial direction than in axial direction, and as the distance increase in the axial direction, the radius of temperature distribution is increase.

According to the state of the flow, the Figure 5(a), (b) and (c) were divided into two groups. Figure 5(a) is the first group and Figure 5(b), (c) are the second group. When the pressure is 2MPa, the state of the flow is laminar. But when the pressure is 10MPa or greater than 10MPa, the velocity of the jet is exceeded 100 m/s, the state of the flow is turbulence. There must be have a threshold pressure which can determine the flow is laminar or turbulence, in this experiment the threshold pressure should less than 10MPa and more than 2MPa. Because of the increment of the pressure, more heat was generated and the temperature of the jet also becomes higher. During the high velocity jet with higher temperature flowing in the air, the radial velocity fluctuation of the jet caused that the mass exchange between the jet and the ambient air and accompanied with heat exchanging. The amount of exchanged mass and heat grow as the radial velocity fluctuation increase.

In the nonisothermal free jet, the process of heat exchanging is a kind of shift of turbulence. Therefore, the similarity of the temperature profile is caused by the similarity of the velocity profile. Figure 6 shows the velocity and temperature distribution of the jet in the radial direction at the different cross-sections of x=10, 40, 70 mm. It can be seen that the velocity profile is similar to the temperature distribution in the radial direction, but the two distributions are not just the same. This finding is consistent with the results of Van der Hegge Zijnen B G. (1958) when he studied the jet in combustion.

5. CONCLUSIONS

Using infrared thermal imager for setting up energy distribution of the jet is a perfect method. The real-time infrared thermal images provide abundant information about the water jet, which can not obtained by others testing methods. Not only can we obtain the temperature profile of the jet, but also the fluctuation of the turbulence can be expressed in the infrared thermal images. The results of the study demonstrated that it is a good way to obtain the mathematical model of the complicated fluid flow by use of the infrared thermal imager and theoretical analysis.

6. ACKNOWLEDGMENT

The authors express sincere thanks to the “Basic Research on the Safety of Major Engineering Projects in Hazardous environments (No.2002CB412700)”, for the financial support, to undertake this research work.

7. REFERENCES

Humio Kiyono, Saito, Sugimoto and Hand, “The Study Regarding a Digging System of a Mortar Sample By a Water Jet,” Journal of the WaterJet Technology Society of Japan, Vol. 7 No 3, 1990.

Shimzu, “The Structure of a WaterJet and Erosion Process of a Material,” Journal of the WaterJet Technology of JAPAN, Vol. 9, No2, 1992.

Bhria, “Jet Cutting Technology,” Proceeding of the 9th International Symposium on Sendai, Japan 4-6 October, 1988.

Masatoshi Hirao, Tianjun Luo, Keiichi Shirase, “The Influence of Water Jet Velocity and Pressure Distribution on Erosion,” FED-Vol, 1996 Fluids Engineering Division Conference Volume 4 ASME 1996.

Hlaváč.L.M., Hlavácová.M.I, Mádr.V., “Quick Method for Determination of the Velocity Profile of the Axial Symmetrical Supersonic Liquid Jet,” Proceeding of the 10th American Waterjet Conference August 14-17, 1999: Houston, Texas.

Liu, H., Wang, R.J., Brownl and Kelson, N., “Computational fluid dynamic (CFD) Simulation of Ultrahigh Velocity Abrasive WaterJet,” Key Engineering Materials, Vols. 233-236 (2002), pp. 477-482.

Launder, B.E, and Spalding, D.B., Lectures in mathematical models of turbulence,” Academic Press, 1972.

Liu, H., Wang, J., Kelson, N., Brown, R.J., “A Study of Abrasive WaterJet Characteristics by CFD Simulation,” Journal of Materials Processing Technology 153-154 (2004) 488-493.

Wang, J., Abrasive WaterJet Machining of Engineering Materials, Trans Tech Publications, Switzerland, 2003.

Pantankar, S.V., Numerical Heat Transfer and Fluid Flow, McGraw Hill Book Company, 1980.

Kovacevic, R., Mohan, R., Beardsley, H., “Monitoring of Thermal Energy Distribution in Abrasive Waterjet Cutting Using Infrafed Thermography,” ASME, Journal of Manufacturing Science and Engineering. 118, pp 555-563. 1996.

Van der Hegge Zijnen B G.: “Appl. Sci. Res,” A.7. pp. 256-276, 1958.

8. NOMENCLATURE

μ Molecular viscosity of the fluid
ε Dissipation rate of the turbulent kinetic energy
σ_k and σ_ε the turbulent Prandtl numbers for k and ε, respectively
ρ_w Density of the water
ρ_g Density of the air
r Diameter of the water jet
x Distance from the nozzle
μ_t Turbulent viscosity
P Pump Pressure (MPa)
u Axial velocity of the water jet
v Radial velocity of the water jet
T Temperature of the water jet
G_k Generation of turbulent kinetic energy due to the mean velocity gradients

9. GRAPHICS

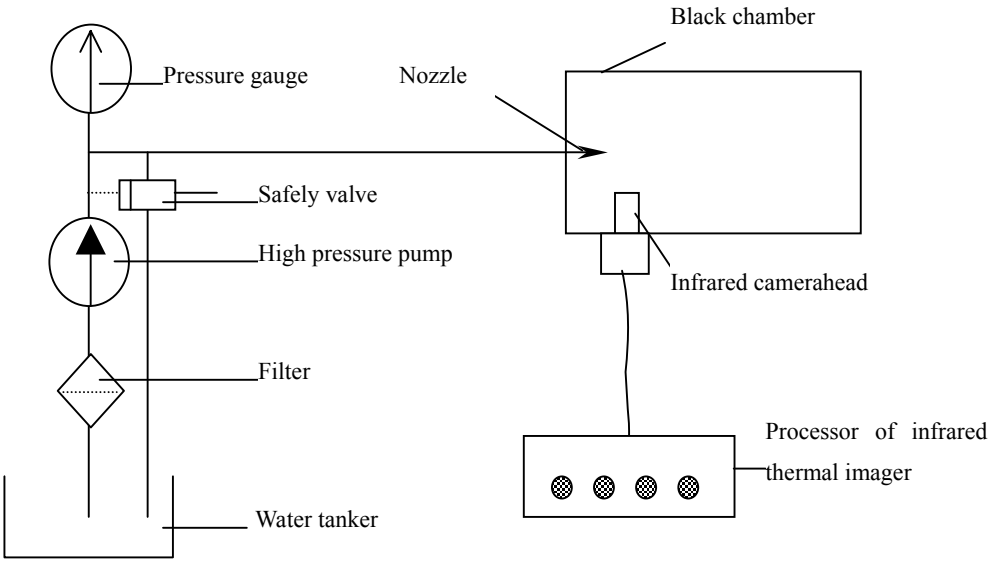

Figure 1. Schematic of Experimental Setup

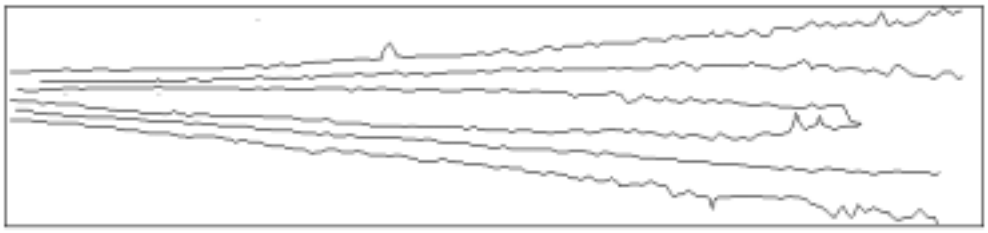

(a) Experimental data

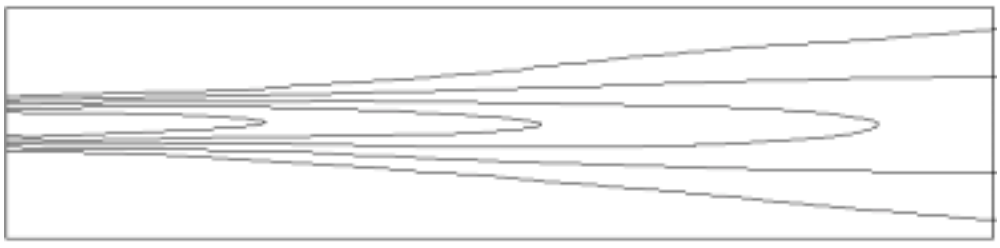

(b) Numerical solutions

Figure 2. Temperature Contours of Water Jet

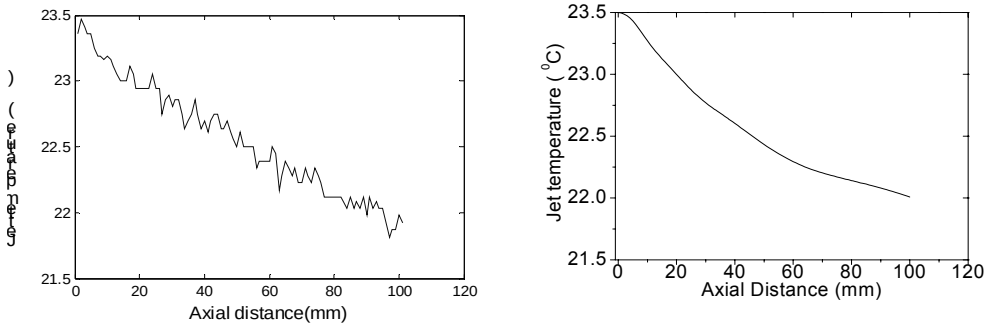

(a) Experimental Data (b) Numerical Data

Figure 3. Temperature Distribution along the Jet Axial Direction (r=0 the centerline of the nozzle)

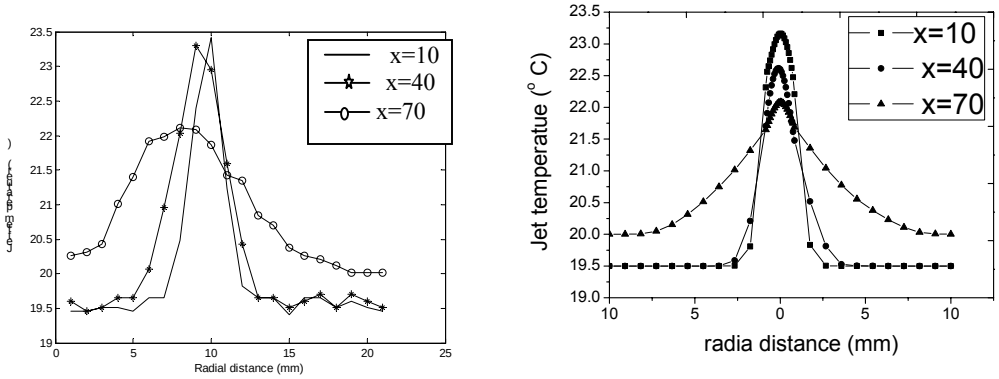

(a) Experimental Data (b) Numerical Data

Figure 4. Radial Profile of Temperature (x= the distance from the nozzle)

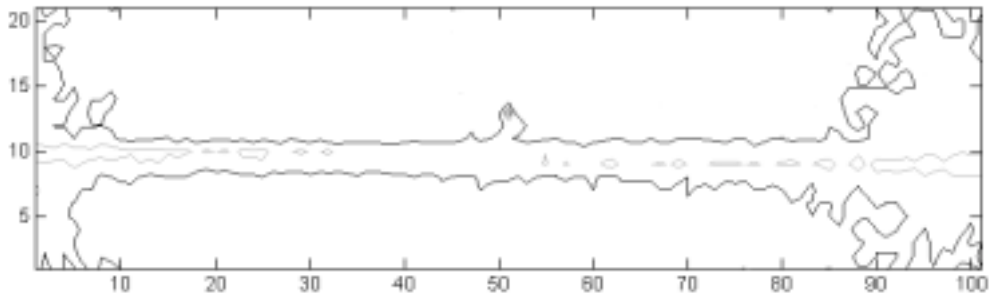

(a) P=2MPa

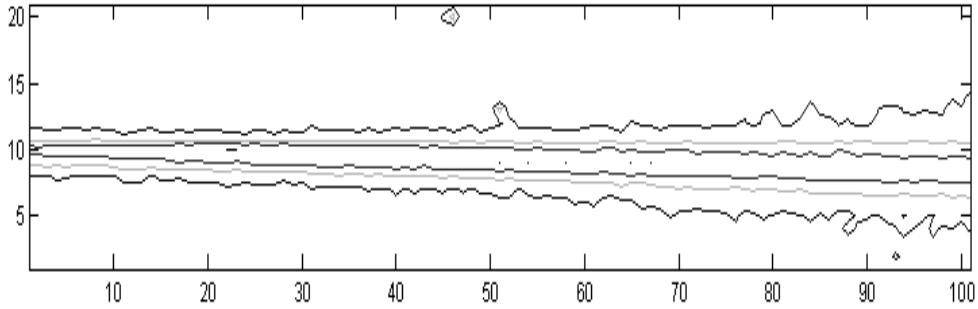

(b) P=10MPa

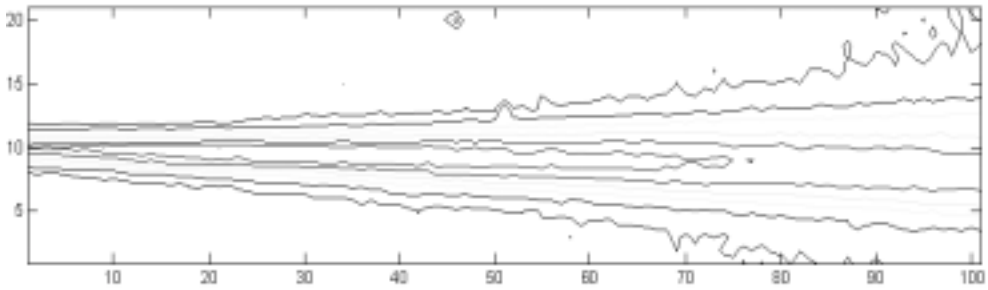

(c) P=30MPa

Figure 5.Temperature Distributions of Jet at Difference Pressure

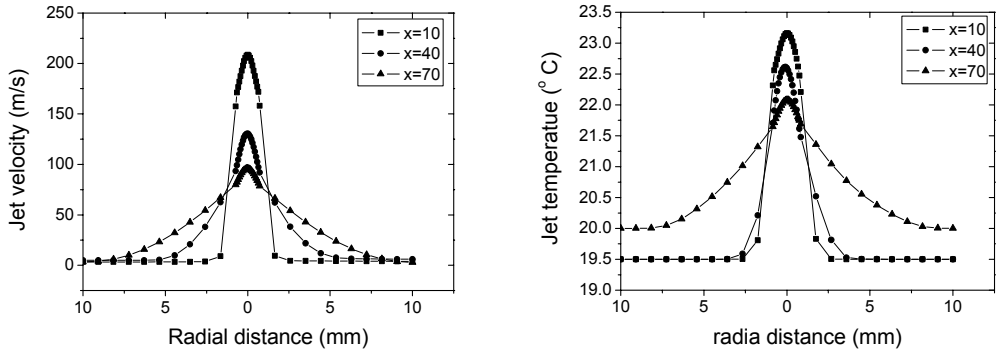

(a) Velocity Profile (b) Temperature Profile

Figure 6. Radial Profile of Velocity and Temperature(x= the distance from the nozzle)